Magnus Attenuation on a Generic Missile Configuration Using N-Vanes

R. L. Kittyle*
Eglin Air Force Base, Florida

The influence of N-vanes on the Magnus moment and dynamic stability of a high-fineness-ratio, spinning, generic missile shape is presented in this paper. Free-flight aeroballistic tests to obtain these data were conducted at atmospheric pressure and over a Mach number range of 1.45–1.76. The aerodynamic coefficients and derivatives presented were extracted from the position/attitude/time histories of the experimentally measured trajectories using nonlinear numerical integration data-reduction routines. Results of this analysis indicate that a dynamic instability due to Magnus exists with the smooth-body configuration but that by using N-vanes, the dynamic stability can be drastically altered. The N-vanes clearly affected the nature of Magnus and, with one configuration, sufficiently weakened the Magnus moment to provide dynamic stability.

Nomenclature

c.g.	= center of gravity
C_ℓ	= roll moment coefficient, $\ell/\bar{q}Ad$
C_{ℓ_p}	= slope of the roll moment vs spin
C_m	= pitching moment coefficient, $m/\bar{q}Ad$
C_{mq}	= pitch damping derivative, $\partial C_m/\partial[qd/2V]$
C_{m_α}	= slope of pitching moment coefficient vs α
$C_{m_{\alpha 3}}, C_{m_{\alpha 5}}$	= cubic and fifth-order pitching moment coefficient derivatives
C_N	= normal force coefficient, $F_N/\bar{q}A$
$C_{N\alpha}$	= slope of the normal force vs α
$C_{N_{\alpha 3}}, C_{N_{\alpha 5}}$	= cubic and fifth-order normal force derivatives
C_{np}	= Magnus moment coefficient
C_{np_α}	= slope of the Magnus moment coefficient vs α
$C_{np_{\alpha 3}}$	= cubic order Magnus moment derivative
C_X	= axial force coefficient, axial force/$\bar{q}A$
C_{X_0}	= axial force coefficient at zero angle of attack
C_{X_M}	= slope of axial force coefficient vs Mach number
C_{yp}	= Magnus force coefficient
L	= model length
ℓ, m, n	= roll, pitch, and yaw moments
$\bar{m}$	= model mass
$\bar{q}$	= dynamic pressure
$\bar{\delta}^2$	= effective angle of attack squared
ω_n	= nutational frequency

Superscripts

$(\dot{})$	= first derivative with respect to time
$(\bar{})$	= total values

Introduction

HIGH length-to-diameter missiles have been of prime importance to munitions, rocket, and missile designers because of compact size and penetration qualities of long-rod kinetic-energy warheads. Yet there are aerodynamic problems associated with these high-fineness-ratio designs. Frequently, to minimize the dispersion effects of structural or thrust asymmetries, initial spin rates are imparted to the configuration. In order to prevent a classic spin-yaw resonant condition ($P = \omega_n$), the missile's roll rate is designed to be several times greater than the nutational frequency. This spin rate does not present a problem at very low angles of attack but, as the angle of attack increases, the spin can prove detrimental to the dynamic stability of the configuration. Associated with spinning missiles at angles of attack is the Magnus force and moment. When present, this force and moment can dominate the dynamics of the system. Because these effects are frequently destabilizing, they cannot be ignored, and methods must be developed to reduce them. Dr. Nicolaides has shown that the use of small longitudinal vanes on spinning bodies can alter Magnus properties.[1] These Nicolaides vanes, referred to as N-vanes, are approximately the height of the boundary layer or smaller and are positioned to redirect the flow.[2,3] If the N-vanes are canted opposite to the circulation, the flow circulation can be reduced or completely reversed, depending on spin rate and vane design.

An early investigation of helical vane effects on a spinning body involved the influence of an engraved rifling band on the aerodynamics of a bullet.[4] An important result of this study was the unexpected alteration of the Magnus moment. Further recent testing on a spin-stabilized body indicates that the damping and Magnus characteristics of a boattailed projectile can be favorably altered by the addition of small fins to the boattail section of the body.[5] Vanes have also been shown to be effective for statically stable bodies. In 1972, vanes added to the nose cone of a dynamically unstable body created a stable configuration.[6] The tests indicate a wide variety of possible applications for N-vanes. This paper will describe the efforts to attenuate the negative effect of Magnus on a generic missile configuration using N-vanes during recent free-flight aerodynamic tests.

Approach

The Magnus force and moment is created through the complex interaction of the freestream air, the circulating boundary layer, and the body vortices. At low angles of attack (α), the force and moment behave linearly, the body vortices are nonexistent, and Magnus is dictated by the cross product of the spin vector and the freestream velocity. At moderate angles, the surface area of the body experiencing the freestream velocity increases, body vortices begin to develop, and the circulation subsequently increases, resulting in a larger Magnus force and moment. With the formation of body vor-

Received June 5, 1986; presented as Paper 86-2082 at the AIAA Atmospheric Flight Mechanics Conference, Williamsburg, VA, Aug. 18–20, 1986; revision submitted Oct. 27, 1986.

*2nd Lt., USAF; Project Engineer, Aeromechanics Div., Air Force Armament Laboratory. Member AIAA.

tices, the Magnus moment variation with α becomes highly nonlinear. At high angles of attack, the boundary layer begins to shift the vortex sheets in the direction of spin, creating a positive Magnus force and moment (Fig. 1). The larger the Magnus moment derivative, the more likely that Magnus will force the system to be dynamically unstable. This characteristic is evident in the dynamic stability parameter.[7]

$$S_d = \frac{2[C_{N\alpha} - C_X + (\bar{m}d^2/2I_x)C_{np_\alpha}]}{C_{N\alpha} - C_X - (\bar{m}d^2/2I_y)C_{mq} + (\bar{m}d^2/2I_x)C_{\ell_p}} \quad (1)$$

The two dominant factors in the dynamic stability relationship [Eq. (1)] for missile configurations are the Magnus moment derivative (C_{np_α}) and the damping-in-pitch derivative (C_{mq}). Since the transverse moment of inertia (I_y) can be several magnitudes larger than the axial moment of inertia (I_x), the C_{np_α} term can have a greater impact on the dynamic stability parameter than C_{mq}. Therefore, reducing the Magnus contribution can be the key to ensuring dynamic stability.

There are two primary approaches to overcoming the effects of Magnus, the first being to determine precisely the Magnus force and moment throughout the flight envelope and then to develop control hardware and software to retain stability. This requires very costly testing and hardware development and is not practical for small, inexpensive munitions. The second approach, and the one documented in this paper, is to develop hardware that can eliminate, or at least attenuate, the Magnus force and moment. Two different N-vane configurations were tested on the generic missile model for this analysis. Additionally, a trip ring was used in place of the vanes to determine if the vanes were merely tripping the flow. The experimental measurements of the vane effects on the missile's free-flight trajectories were obtained in a free-flight spark range.[8]

Models and Test Conditions

The overall model geometry is shown in the sketches of Fig. 2. To approximate a modern high-fineness-ratio missile, an L/D of 30 was chosen. A brass von Kármán ogive nose and a simple flare aft were used to stabilize the configuration with a minimum static margin of 1.5% of the body length. Two N-vane configurations were tested on the model, one with 18 vanes and the other with 9 vanes. Each set of vanes was canted at 22 deg off centerline in the direction to counter-rotate the circulation. These vanes were located at 60% of the body length from the nose. Additionally, to test whether the vanes were actually turning and not just tripping the flow, an additional model containing a solid trip ring, with the same height as the vanes, was also tested.

Fifteen models were flown in the spark range during the test program; nine flights were completely successful, the measured trajectories were analyzed, and the aerodynamic coefficients and derivatives were extracted. The tests were conducted at atmospheric pressure over a Mach number range of 1.45-1.76. The measured physical properties of each model and the associated test conditions for each of the nine flights successfully analyzed are presented in Table 1.

The models were launched from a rifled 30-mm ID propellant gun using a two-piece sabot. No attempt was made to augment the initial angular disturbances of the models as the model/sabot package exited the launcher.

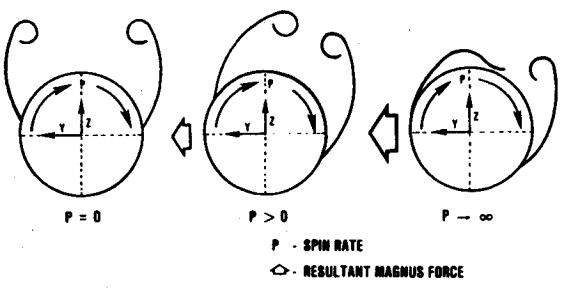

Fig. 1 Magnus at high angles of attack (rear view).

Free-Flight Data Reduction

Extraction of the aerodynamic coefficients and derivatives is the primary goal in analyzing the trajectories measured in free flight. This is accomplished by using the Aeroballistic Data Analysis System,[9] which incorporates a standard linear theory analysis[10] and a six degree-of-freedom (6-DOF) numerical integration technique.[11]

The aerodynamic parameters are fit to match the experimental trajectories using the maximum likelihood method.[8] This is an iterative procedure that adjusts the aerodynamic model coefficients to maximize the probability that the calculated state trajectory will match the measured state. Initially, the flight of each model was analyzed separately; then the flights of the same configurations were simultaneously analyzed using the 6-DOF multiple-fit technique. This provides a common set of aerodynamics that matched each of the separately measured position/attitude/time profiles. The multiple-fit approach provides a more complete range of angle-of-attack and roll-orientation combinations than would be available from any one flight considered independently. This increases the probability that the determined coefficients define the model's aerodynamics over the entire range of test conditions.

Aerodynamic Model

The aerodynamic data presented in this paper were obtained using the fixed plane 6-DOF analysis.[12] The equations of motion are derived with respect to a fixed-plane coordinate system: the x-axis extends downrange, the y-axis points to the left when looking downrange, and the z-axis extends upward. The 6-DOF differential equations of motion in this system are listed in detail in Ref. 13. The solution of the equations define the flight motion of a symmetric missile in fixed-plane coordinates. Since the position/attitude measurements, as acquired from a ballistic spark range, are obtained with respect to an Earth-fixed axis system, additional transformations are required. The transformation equations, also shown in Ref. 11, are in terms of the fixed-plane Euler angles (θ, ψ) and the angle of rotation about the missile axis (ϕ). Coriolis accelerations are also accounted for in the 6-DOF equations. A fourth-order Runge-Kutta scheme is used to integrate the equations of motion numerically.

The basic definitions of the aerodynamic forces and moments as used in the 6-DOF program follow:

$$F_x = -\bar{q}A\bar{C}_X \quad (2)$$

$$F_y = \bar{q}A\left[-\bar{C}_{N\alpha}\frac{v}{V} + \frac{pd}{2V}\bar{C}_{Yp\alpha}\frac{w}{V} + \bar{C}_{Y\gamma\alpha}\frac{w}{V}\right.$$

$$\left. + C_{N\delta}\delta_A \sin\phi - \bar{C}_{N\delta}\delta_B \cos\phi\right] \quad (3)$$

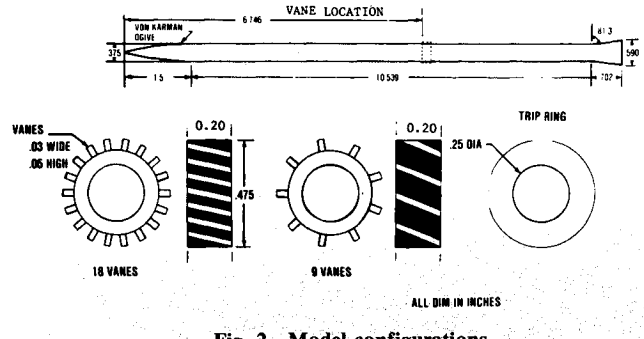

Fig. 2 Model configurations.

$$F_z = \bar{q}A\left[-\bar{C}_{N\alpha}\frac{w}{V} - \frac{pd}{2V}\bar{C}_{Yp\alpha}\frac{v}{V} - \bar{C}_{Y\gamma\alpha}\frac{v}{V}\right.$$

$$\left. - C_{N\delta}\delta_A\cos\phi - \bar{C}_{N\delta}\delta_B\sin\phi\right] \quad (4)$$

$$\ell = \bar{q}Ad\left[\frac{pd}{2V}\bar{C}_{\ell_p} + \bar{C}_{\ell}\right] \quad (5)$$

$$m = \bar{q}Ad\left[\bar{C}_{m_\alpha}\frac{w}{V} + \frac{qd}{2V}\bar{C}_{mq} + \frac{pd}{2V}\bar{C}_{np_\alpha}\frac{v}{V} + \bar{C}_{n_\alpha}\frac{v}{V}\right.$$

$$\left. + \bar{C}_{n\gamma\alpha}\frac{v}{V} + \bar{C}_{m\delta}\delta_A\cos\phi - \bar{C}_{m\delta}\delta_B\sin\phi + RMQ\right] \quad (6)$$

$$n = \bar{q}Ad\left[-\bar{C}_{m_\alpha}\frac{v}{V} + \frac{rd}{2V}\bar{C}_{mq} + \frac{pd}{2V}\bar{C}_{np_\alpha}\frac{w}{V} + \bar{C}_{n_\alpha}\frac{w}{V}\right.$$

$$\left. + \bar{C}_{n\gamma\alpha}\frac{w}{V} + \bar{C}_{m\delta}\delta_A\sin\phi + \bar{C}_{m\delta}\delta_B\cos\phi + RNQ\right] \quad (7)$$

The aerodynamic parameters shown in Eqs. (2-7) are expanded as functions of Mach number, sine of the total angle of attack (ϵ), and the aerodynamic roll angle (γ). These expansions are shown in detail as Eqs. (8-22).

$$\bar{C}_X = C_{X_0} + C_{X\bar{\alpha}_2}\epsilon^2 + C_{X\bar{\alpha}_4}\epsilon^4 + C_{X_M}(M_i - M_r)$$

$$+ C_{X\gamma\bar{\alpha}_2}\epsilon^2\cos N\gamma \quad (8)$$

$$\bar{C}_{N\alpha} = C_{N\bar{\alpha}} + C_{N\bar{\alpha}_3}\epsilon^2 + C_{N\bar{\alpha}_5}\epsilon^4 + C_{N\gamma\bar{\alpha}_3}\epsilon^2\cos N\gamma$$

$$+ C_{N\bar{\alpha}M}(M_i - M_r) \quad (9)$$

$$\bar{C}_{N\delta}\delta_A = C_{N\delta}\delta_A \quad (10)$$

$$\bar{C}_{N\delta}\delta_B = C_{N\delta}\delta_B \quad (11)$$

$$\bar{C}_{Yp\alpha} = C_{Yp\bar{\alpha}} + C_{Yp\bar{\alpha}_3}\epsilon^2 \quad (12)$$

$$\bar{C}_{Y\gamma\alpha} = C_{Y\delta\bar{\alpha}_3}\epsilon^2\sin N\gamma \quad (13)$$

$$\bar{C}_{\ell_p} = C_{\ell_p} + C_{\ell p\bar{\alpha}_2}\epsilon^2 + C_{\ell_{pM}}(M_i - M_r) \quad (14)$$

$$\bar{C}_{\ell} = \bar{C}_{\ell\delta}\delta + C_{\ell\gamma\bar{\alpha}_2}\epsilon^2\sin N\gamma \quad (15)$$

$$\bar{C}_{m\alpha} = C_{m\bar{\alpha}} + C_{m\bar{\alpha}_3}\epsilon^2 + C_{m\bar{\alpha}_5}\epsilon^4 + C_{m\alpha M}(M_i - M_r)$$

$$+ C_{m\gamma\bar{\alpha}}\cos N\gamma + \bar{C}_{N\bar{\alpha}}(CG - CG_r) + C_{m\gamma\bar{\alpha}_3}\epsilon^2\cos N\gamma \quad (16)$$

$$\bar{C}_{mq} = C_{mq} + C_{mq\bar{\alpha}_2}\epsilon^2 + C_{mq\bar{\alpha}_4}\epsilon^4 \quad (17)$$

$$\bar{C}_{np\alpha} = C_{np\bar{\alpha}} + C_{np\bar{\alpha}_3}\epsilon^2 + C_{np\bar{\alpha}_5}\epsilon^4 + C_{np\bar{\alpha}_7}\epsilon^6 \quad (18)$$

$$\bar{C}_{n\alpha} = C_{n\bar{\alpha}} \quad (19)$$

$$\bar{C}_{n\gamma\alpha} = C_{n\gamma\bar{\alpha}}\sin N\gamma + C_{n\gamma\bar{\alpha}_3}\epsilon^2\sin N\gamma \quad (20)$$

$$\bar{C}_{m\delta}\delta_A = C_{m\delta}\delta_A \quad (21)$$

$$\bar{C}_{m\delta}\delta_B = C_{m\delta}\delta_B \quad (22)$$

The aerodynamic roll angle is computed by transforming the fixed-plane velocities into the rolling-body coordinate system as follows:

$$v_b = v\cos\phi + w\sin\phi \quad (23)$$

$$w_b = -v\sin\phi + w\cos\phi \quad (24)$$

$$\gamma = \tan^{-1}(v_b/w_b) \quad (25)$$

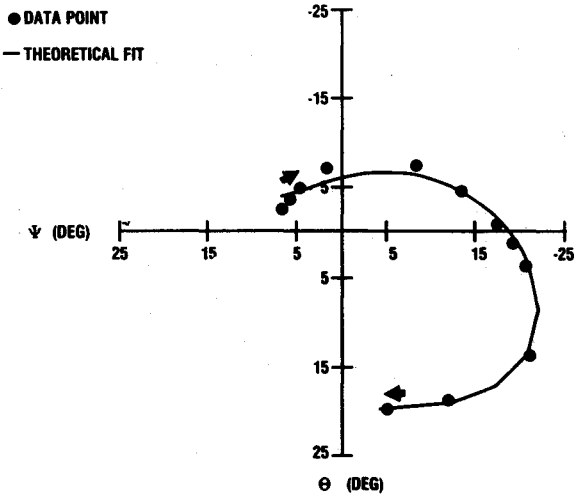

Fig. 3 Typical angular motion plot of the basic configuration, aft c.g.

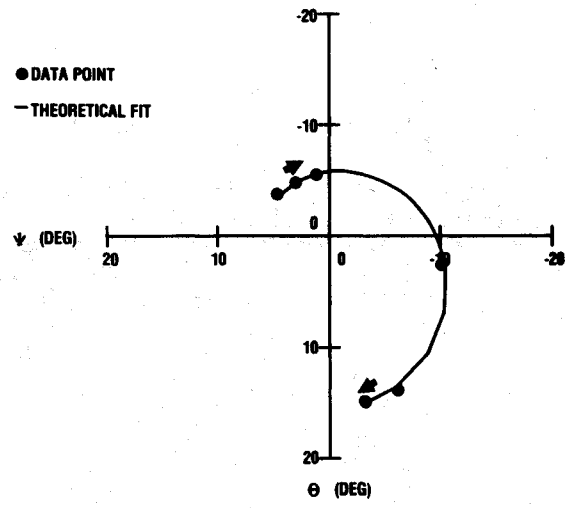

Fig. 4 Typical angular motion plot of the basic configuration, forward c.g.

Results and Discussion

Qualitative

The trajectory of the basic configuration was established first. As seen in Fig. 3, this configuration immediately diverged to a 22-25-deg nutational limit cycle. The Magnus moment overwhelmed the system dynamics and prevented any pitch damping.

The N-vanes on the vaned models proved very fragile and frequently broke during the launch phase. Additionally, the aerodynamic frequencies of the vaned models tended to resonate with a structural frequency, causing model failure. To prevent the frequency matching, the aerodynamic frequencies were increased by moving the c.g. forward. Two more basic models with the c.g. shifted forward were subsequently launched. A typical trajectory of these flights is depicted in Fig. 4.

Only two of the four 18 vane models launched provided useful data. It is interesting that whereas the basic configuration demonstrated a nutational instability, the 18 vane models

were precessionally undamped. Figure 5 shows the counterclockwise angular motion spiral that characterized these flights.

Only a single 9 vane model survived launching and gave useful data. The angular motion pattern of this flight is depicted in Fig. 6. The model received a substantial initial angle of attack, yet it clearly begins to damp. These flights indicate that N-vanes can alter the missile's inherent Magnus characteristics and that a vane design exists which provides favorable dynamic stability to the system.

The angular motion of the trip ring configuration was not similar to the vaned models (Fig. 7). This flight exhibits a nutational instability more akin to the basic configurations than the vaned ones. This flight indicates that the vanes are not just tripping the flow but are altering the circulation in some other manner.

Quantitative

Using a 6-DOF data analysis code incorporating the maximum likelihood method, the aerodynamic coefficients and derivatives were extracted for the different configurations (Table 2). As would be expected of these high angle of attack trajectories, most of the coefficients were nonlinear with respect to α. For the basic and 18 vane configurations, a cubic Magnus moment derivative expansion was used, and a fifth-order pitch moment derivative was required to fit the equations of motion to the experimental trajectories.

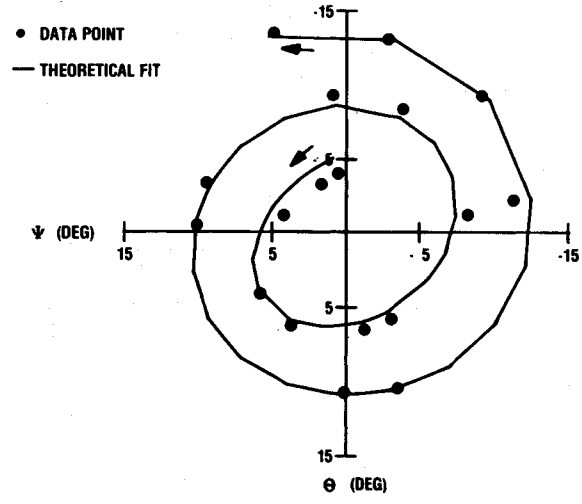

Fig. 5 Typical angular motion plot of the 18 vane configuration.

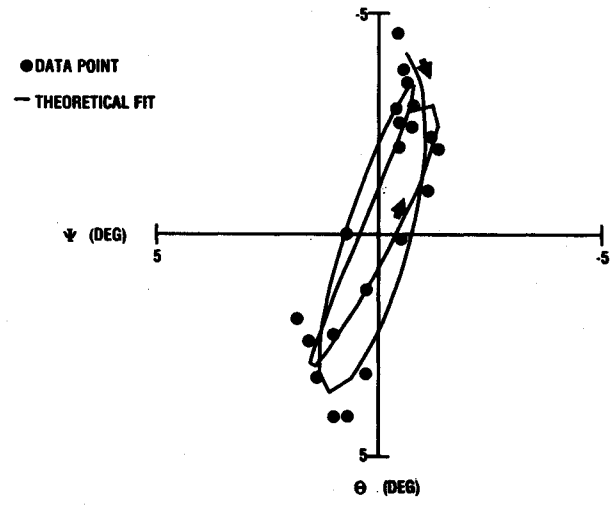

Fig. 6 Angular motion plot of the 9 vane configuration.

Table 1 Physical properties and test conditions

Shot no.	Configuration	Mach no.	Re_L, $\times 10^{-6}$	δ^2, deg^2	Mass, gm	$X_{c.g.}/L$ (from nose)
35	Basic	1.45	9.413	243.2	63.14	.465 (aft c.g.)
36	Basic	1.508	9.900	296.8	63.41	.466 (aft c.g.)
37	Basic	1.56	10.236	256.5	63.08	.466 (aft c.g.)
42	18 vane	1.59	10.354	14.1	57.0	.429 (forward c.g.)
43	18 vane	1.57	10.120	93.0	56.67	.429 (forward c.g.)
44	9 vane	1.76	11.362	7.0	56.91	.429 (forward c.g.)
45	Trip ring	1.535	10.053	307.7	57.12	.434 (forward c.g.)
48	Basic	1.49	9.624	2.7	56.03	.427 (forward c.g.)
49	Basic	1.52	9.816	114.9	55.71	.423 (forward c.g.)

Table 2 6-DOF fit results

Shot no.	Mach no.	C_{X_0}, $C_{X_{\alpha 2}}$, C_{X_M}	C_{N_α}, $C_{N_{\alpha 3}}$	$C_{y_{p_\alpha}}$, $C_{n_{p_\alpha}}$, $C_{n_{p_{\alpha 3}}}$	C_{m_α}, $C_{m_{\alpha 3}}$, $C_{m_{\alpha 5}}$	C_{m_q}, C_{l_p}
35, 36, 37	1.504	1.108	7.00	−186.03	−3.18	−2000.0
(basic, aft c.g.)		2.000	79.93	781.99	−88.28	−.1
		−.200		−4507.80	274.30	
48, 49	1.508	1.156	6.85	−89.92	−37.44	−2000.0
(basic, forward c.g.)		2.000	62.25	−353.60	381.19	−.1
		−.200		93092.00	0.0	
42, 43	1.580	1.477	7.20	22.59	−25.25	−2000.0
(18 vanes)		2.000	83.03	−483.73	−263.91	−.1
		−.200		5785.40	0.0	
44	1.760	1.101	7.73	0.0	−24.31	−3000.0
(9 vanes)		2.000	0.0	−136.98	0.0	−.1
		−.200		0.0	0.0	

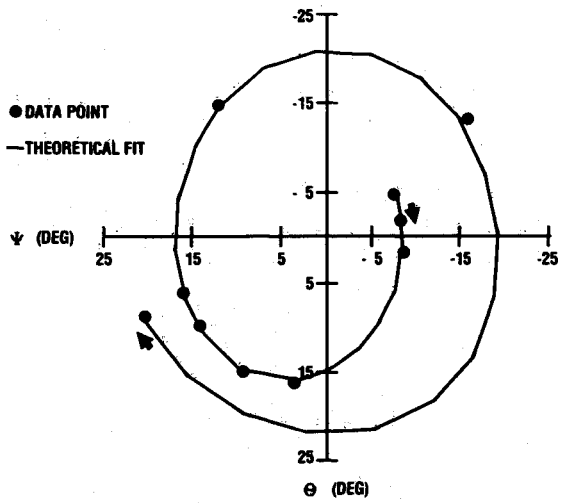

Fig. 7 Angular motion plot of the trip ring configuration.

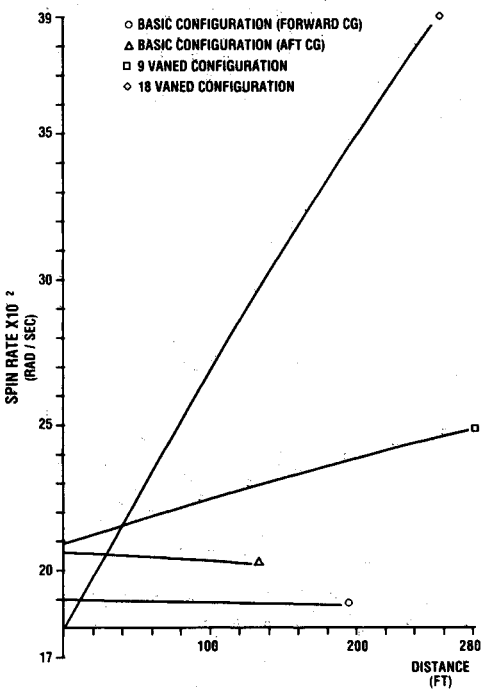

Fig. 8 Spin rates.

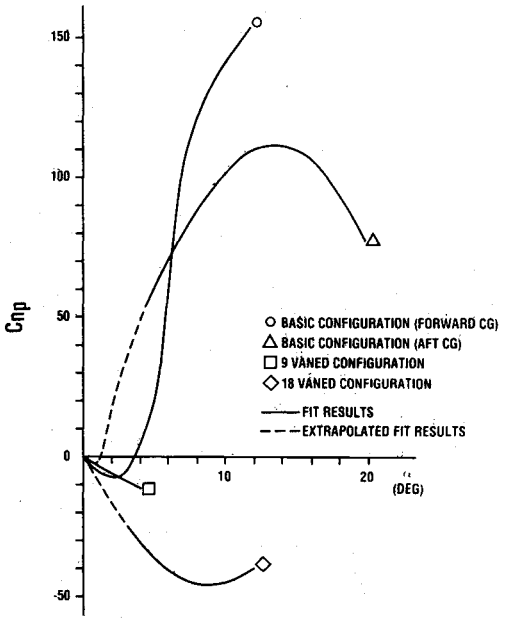

Fig. 9 Magnus moment coefficients.

One of the most difficult parameters to determine was the pitch damping derivative C_{mq}. The 9 vane configuration readily approached a C_{mq} value of -3000, yet the resultant fit coefficients were relatively insensitive to variations in C_{mq} of up to ± 1000. The 18 vane configurations approached a value of -2000 for C_{mq}, but there were negligible differences (less than 3%) to the trajectory fits when C_{mq} values of -3000 or -1000 were used. The fits of the basic configurations originally resulted in positive values for the pitch damping derivative. When it was clear that the dynamic instability probably was not caused by a pitch driving moment but was more likely to result from the out-of-plane Magnus moment, C_{mq} was held constant at -2000. Since the trajectory fit improved by more than 5%, indications are that a negative C_{mq} was in order. This demonstrates a long-standing problem associated with data-reduction codes, where the program can have difficulty distinguishing between a dynamic instability due to a Magnus moment derivative or one caused by a positive C_{mq}. The same type of problem was encountered when fitting the roll motion. Both basic configurations fit a roll damping derivative of -0.1/rad with an uncertainty of 50% so each C_{ℓ_p} was held constant at -0.1/rad. The vaned models had increasing roll rates so they could not fit a negative roll damping derivative, even when allowing for a roll driving moment. A C_{ℓ_p} value of -1.0 was subsequently held constant for the trajectory fits of the 18 vane and 9 vane models with satisfactory results. Additionally, the axial force derivative with respect to Mach number was not fit in any configuration because there were not sufficient Mach number variations between the launches.

The most interesting results of this test program came from evaluating the effectiveness of the N-vanes at turning the circulation. In order to turn the flow, a torque is imparted to the model through the vanes. This torque is in the same direction as spin, so a greater torque results in a greater spin rate. Figure 8 plots the spin rates vs downrange distances of the various configurations. The basic configurations behave typically of spinning bodies without roll driving moments (i.e., the roll rates decrease due to the roll damping derivative C_{ℓ_p}). The 18 vane models clearly show the effects of the vane torque by significant increases in roll rate. This indicates that the boundary-layer flow is not being choked between the vanes nor is the flow simply being tripped. The 18 vanes are effectively turning the flow and simultaneously increasing the spin rate. The 9 vane model also impart a torque yet not the extent of the former. It is important to note that the vanes were effective in turning the circulation and that their effects on the Magnus moment are consistent with the increasing roll rates.

The Magnus moment coefficient vs α is depicted in Fig. 9. This graph dramatically portrays the impact N-vanes have on the Magnus moment. The basic configuration with the aft c.g. did not provide data lower than 5 deg, but the slope of C_{np} at 5 deg and higher is quite large and easily accounts for the dynamic instability of this model. By moving the c.g. forward on the basic configuration, the Magnus moment is simply increased because of the larger moment arm from the Magnus center of pressure to the model c.g. The 18 vane models have conversely forced the Magnus moment derivative to relatively high negative values. These vanes have overcorrected the flow and have reversed the circulation. The 9 vane configuration has also reversed the flow, though not as much. To determine the influence of these Magnus moment changes on the dynamic stability of the models, a dynamic stability chart is employed.

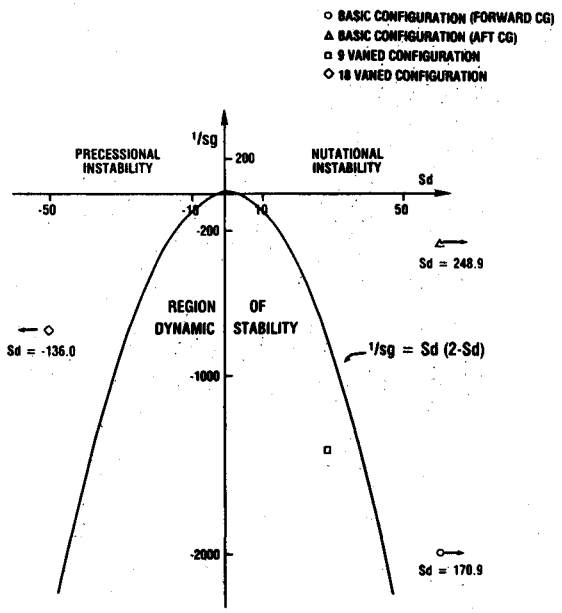

Fig. 10 Dynamic stability plot.

Using Eq. (1) and the following relationship for the inverse of the gyroscopic stability factor, a region can be defined where configurations are dynamically stable.[7]

$$1/S_g = \pi\rho I_y C_{m\alpha} d^3 V^2 / 2I_x^2 P^2 \tag{26}$$

Figure 10 shows the region of stability along with the locations for the test configurations at 3.5-deg angle of attack. As expected, the basic model with the aft c.g. was nutationally unstable and considerably far from the stable region. The basic configuration with the forward c.g. was much lower on the $1/S_g$ axis due to the larger magnitude of C_{m_α}, but it is similarly far from the realm of dynamic stability. The true indication of the potential of N-vanes for attenuating Magnus is the location of the 18 vane and 9 vane models. The 18 vane model brought the configuration through the region of dynamic stability and excessively turned the circulation into the reverse direction. This changed the direction of the Magnus moment but did not reduce the magnitude sufficiently. Consequently, the 18 vane models were precessionally unstable. The 9 vane model provided a compromise between the two extremes and falls in the dynamic stability region. This combination of vanes and vane cant angle sufficiently attenuated the circulation, which in turn reduced the Magnus moment derivative, enabling the configuration to be dynamically stable.

Conclusions

The use of N-vanes as an anti-Magnus device demonstrates considerable potential. N-vanes can greatly increase the utility of high-fineness-ratio spinning munitions not only by improved dynamic stability, but also for missile maneuverability. Because the Magnus moment is formed through the complex interaction of the boundary layer, the freestream velocity, and body vortices, it appears that testing is required to determine how many vanes, at what height, and what vane cant angle will adequately attenuate the circulation. By the correct choice of a set of N-vanes, the circulating boundary layer can be weakened and the Magnus effects controlled.

References

[1]Ingram, C. W., Lusardi, R. J., and Nicolaides, J. D., "Effects of Rifling and N-Vanes on the Magnus Characteristics of Bodies of Revolution," AIAA Paper 72-970, Sept. 1972.

[2]Jenke, L. M., "Experimental Magnus Characteristics of Ballistic Projectiles With and Without Anti-Magnus Vanes at Mach Numbers 1.5 through 2.5," AFATL-TR-73-188, Dec. 1973.

[3]Sears, E. S., "A Method for Eliminating the Magnus Instability of a Finned Missile," AFATL-TR-71-149, Nov. 1971.

[4]Sylvester, M. A. and Braun, W. F., "The Influence of Helical Serrations and Bullet Engraving on the Aerodynamic and Stability Properties of a Body of Revolution with Spin," AIAA Paper 70-557, 1970.

[5]Kline, R. W., "On the Aerodynamic Stabilization of Long, Low Drag Bodies of Revolution Using N-Vanes," Master's Thesis, University of Notre Dame, Notre Dame, IN, June 1971.

[6]Ingram, C. W., Lando, D. W., and Nicolaides, J. D., "The Effects of Anti-Magnus Devices on Fin Bodies and Projectiles," Paper, 9th Navy Symposium on Aeroballistics, May 9-11, John Hopkins University, MD, 1972.

[7]Murphy, C. H., "Free Flight Motion of Symmetric Missiles," U.S. Army Ballistic Research Laboratory, Aberdeen, MD, BRL Rept. 1216, July 1963.

[8]Winchenbach, G. L., Galanos, D. G., Kleist, J. S., and Lucas, B. F., "Description and Capabilities of the Aeroballistic Research Facility," AFATL-TR-78-14, April 1978.

[9]Whyte, R. H., Winchenbach, G. L., and Hathaway, W. H., "Subsonic Free-Flight Data for a Complex Asymmetric Missile," *Journal of Guidance, Control and Dynamics*, Vol. 4, Jan.-Feb. 1981, pp. 59-65.

[10]Murphy, C. H., "Data Reduction for the Free-Flight Spark Ranges," U.S. Army Ballistic Research Laboratory, Aberdeen, MD, BRL Rept. 900, Feb. 1954.

[11]Chapman, G. T. and Kirk, D. B., "A Method for Extracting Aerodynamic Coefficients from Free-Flight Data," *AIAA Journal*, Vol. 8, April 1970, pp. 753-757.

[12]Winchenbach, G. L., Uselton, R. L., Hathaway, W. H., and Chelekis, R. M., "Free-Flight and Wind Tunnel Data for a Generic Fighter Configuration," *Journal of Aircraft*, Vol. 21, Jan. 1984, pp. 5-13.

[13]Whyte, R. H., Hathaway, W. H., Buff, R. S., and Winchenbach, G. L., "Subsonic and Transonic Aerodynamics of Wraparound Fin Configuration," AIAA Paper 85-0106, 1985.